

Cai, D., Henehan, M., Uhlig, D., von
Blanckenburg, F. (2022): Mg isotope
composition of runoff is buffered by the
regolith exchangeable pool. - *Geochimica et
Cosmochimica Acta*, 321, 99-114.

<https://doi.org/10.1016/j.gca.2022.01.011>

Mg isotope composition of runoff is buffered by the regolith exchangeable pool

Di Cai¹, Michael J. Henehan¹, David Uhlig², Friedhelm von Blanckenburg¹

4

¹ GFZ German Research Centre for Geosciences; Section 3.3 Earth Surface Geochemistry; Telegrafenberg, 14473 Potsdam, Germany

² Forschungszentrum Jülich GmbH, Institute of Bio- and Geosciences (IBG-3), Agrosphere, Wilhelm-Johnen-Str, 52425 Jülich, Germany

*Correspondence to: dcai@gfz-potsdam.de

10

Abstract

12 In a small, forested catchment underlain by gneiss (Conventwald, Black Forest, Germany), we
13 found that the magnesium isotope composition ($\delta^{26}\text{Mg}$) of creek water did not show seasonal
14 variability, despite variations in dissolved Mg concentrations. To investigate the potential
15 controlling factors on water $\delta^{26}\text{Mg}$ values, we studied the Mg isotope composition of solid samples
16 (bedrock, bulk soil, clay-sized fraction of soil, separated minerals, the exchangeable fraction of
17 regolith) and water samples comprising time series of creek water, groundwater and subsurface
18 flow. Subsurface flow from 0-15 cm depth ($-0.80 \pm 0.08 \text{‰}$) and 15-150 cm depth ($-0.66 \pm 0.17 \text{‰}$),
19 groundwater ($-0.55 \pm 0.03 \text{‰}$), and creek water ($-0.54 \pm 0.04 \text{‰}$) are all depleted in heavy Mg
20 isotopes compared to bedrock ($-0.21 \pm 0.05 \text{‰}$). Subsurface flow samples have similar $\delta^{26}\text{Mg}$
21 values to the regolith exchangeable fraction at the respective sampling depths. Also, groundwater
22 and creek water show $\delta^{26}\text{Mg}$ values that are identical to those of the exchangeable fraction in the
23 deep regolith. We suggest, therefore, that cation-exchange processes in the regolith control Mg
24 concentrations and $\delta^{26}\text{Mg}$ values of creek water at our study site. This assumption was further
25 verified by batch adsorption-desorption experiments using soil samples from this study, which
26 showed negligible Mg isotope fractionation during adsorption-desorption. We propose that the
27 exchangeable fraction of the regolith buffers dissolved Mg concentrations by adsorbing and storing
28 Mg when soil solutions are high in concentration in the dry season and desorbing Mg when rainfall
29 infiltrates and percolates through the regolith in the wet season. This mechanism may explain the
30 near chemostatic behavior of Mg concentrations and the invariance of $\delta^{26}\text{Mg}$ values in creek water.

31 In addition, the depth distribution of exchangeable Mg concentration and isotope composition in
32 the regolith reflects mineral dissolution and secondary mineral formation in deep regolith (> 3 m)
33 and biological cycling in shallower depth (0 – 3m). Magnesium stable isotopes thus provide an
34 accurate snapshot of the geogenic (weathering) and the organic (bio-cycled) nutrient cycle.

35 **1. Introduction**

36 Magnesium (Mg) is a major element in the interior of the Earth and at its surface, the terrestrial
37 hydrosphere, the oceans, and is intensely cycled from the pedosphere into the biosphere. The use
38 of Mg stable isotopes as a tracer to decipher biogeochemical processes in natural systems has
39 evolved in the last two decades into a powerful tool (e.g., Schmitt et al., 2012; Teng, 2017),
40 especially in the Critical Zone - the boundary layer of the Earth that extends from the vegetation
41 canopy down to groundwater.

42

43 Laboratory experiments have documented Mg isotope fractionation by both biotic and abiotic
44 processes. Uptake of Mg by plants generally favors heavy Mg isotopes, and Mg translocation within
45 plants can further fractionate Mg isotopes, as demonstrated in growth experiments (Black et al.,
46 2008; Bolou-Bi et al., 2010) and in field studies (e.g., Bolou-Bi et al., 2012; Uhlig et al., 2017).
47 Mycorrhizal fungi associated with the roots might fractionate Mg isotopes too, as evidenced by
48 fungi growth experiments (Fahad et al., 2016; Pokharel et al., 2017). Not all studies observe such
49 fractionations, however, with some studies indicating negligible Mg isotope fractionation during
50 plant uptake (Mavromatis et al., 2014; Kimmig et al., 2018). Abiotic processes are also capable of
51 fractionating Mg isotopes significantly. For example, during the dissolution of olivine, lighter Mg
52 isotopes are preferentially leached at the initial stage of dissolution (Wimpenny et al., 2010; Maher
53 et al., 2016; Pokharel et al., 2019). Granite dissolution experiments show preferential dissolution
54 of isotopically distinct primary minerals (Ryu et al., 2011). During the formation of secondary
55 minerals, some experimental syntheses of brucite (an analogue of octahedrally-coordinated Mg
56 clays), lizardite and kerolite found heavy Mg isotopes to be preferentially incorporated into the
57 octahedral sites (Wimpenny et al., 2014; Ryu et al., 2016). In contrast, elsewhere brucite (Li et al.,
58 2014), and stevensite and saponite (Hindshaw et al., 2020) were found to favor light Mg isotopes.
59 This variable direction of Mg isotope fractionation is thought to be controlled by Mg-O bond length
60 in clay octahedral sites, although a kinetic effect cannot be ruled out (Li et al., 2014; Hindshaw et
61 al., 2020). Compared to the aforementioned processes, less well documented is whether Mg
62 isotopes fractionate during adsorption-desorption processes. In an adsorption experiment
63 (Wimpenny et al., 2014), Mg retained by clays had almost identical or by only ~0.1‰ more

64 negative $\delta^{26}\text{Mg}$ values than the original Mg solution, suggesting the adsorption of Mg onto clays is
65 associated with little or no Mg isotope fractionation. Similarly, after synthesis of stevensite and
66 saponite, Hindshaw et al., (2020) observed the exchangeable Mg of the synthesized mineral to have
67 a $\delta^{26}\text{Mg}$ value lower than, or within analytical uncertainty of, the initial solution.

68

69 As with these lab experiments under controlled conditions, the Mg isotope composition of river
70 water show similar complexity. For example, river water has been found to be isotopically lighter
71 than the silicate bedrock it drains due to secondary mineral formation favoring heavy Mg isotopes
72 (Tipper et al., 2006a, b, 2008; Brenot et al., 2008; Ma et al., 2015; Dessert et al., 2015). Conversely,
73 however, in other catchments secondary mineral formation incorporating isotopically light Mg is
74 inferred (Pogge von Strandmann et al., 2008). Since aforementioned lab experiments have
75 identified both fractionation directions during secondary mineral formation (e.g., Wimpenny et al.,
76 2014; Li et al., 2014; Hindshaw et al., 2020), these hypotheses are not incompatible. There have
77 also been cases where isotopic fractionation in rivers could not be attributed to the formation of
78 secondary minerals. For example, in Greenland, river water was found to be too dilute to form
79 secondary minerals. Instead, the negative $\delta^{26}\text{Mg}$ values in river water were explained by the
80 preferential dissolution of isotopically light calcite (Wimpenny et al., 2011). Elsewhere, in the
81 Southern Sierra Nevada Critical Zone Observatory (SSCZO) creek water was enriched in light Mg
82 isotopes despite the fact that Mg isotope composition of soil was similar to that of bedrock, which
83 was attributed to the preferential uptake of heavy Mg isotopes by plants (Uhlig et al., 2017).

84

85 Given the complexity of natural watersheds (that vary in lithology, climate and vegetation cover),
86 conclusions drawn from field studies can be more useful if a particular one controlling factor can
87 be singled out. To this end, time series of water samples can be used (e.g., Tipper et al., 2012). Such
88 time series water samples could be collected over discrete storm events (Chapela Lara et al., 2017;
89 Fries et al., 2019) such that short-term hydrological change is the main factor driving variation.
90 Alternatively, they can be collected in different seasons (Bolou-Bi et al., 2012; Tipper et al., 2012;
91 Mavromatis et al., 2014; Uhlig et al., 2017; Hindshaw et al., 2019; Novak et al., 2021) to investigate
92 biological and longer-term hydrological effects. However, the response of $\delta^{26}\text{Mg}$ values to
93 discharge varies among studies. In the studies of Fries et al. (2019) and Hindshaw et al. (2019), Mg
94 concentration and isotope composition changed little compared to discharge variation, while in
95 other studies (e.g., Bolou-Bi et al., 2012; Mavromatis et al., 2014) a clear correlation was found
96 between discharge and $\delta^{26}\text{Mg}$ values. At the event-scale or over a hydrological season, variations
97 in the Mg isotope composition of river water were either attributed to in-stream mixing of Mg from

98 different depths or the combined effect of more than one process (Tipper et al., 2012; Mavromatis
99 et al., 2014; Chapela Lara et al., 2017).

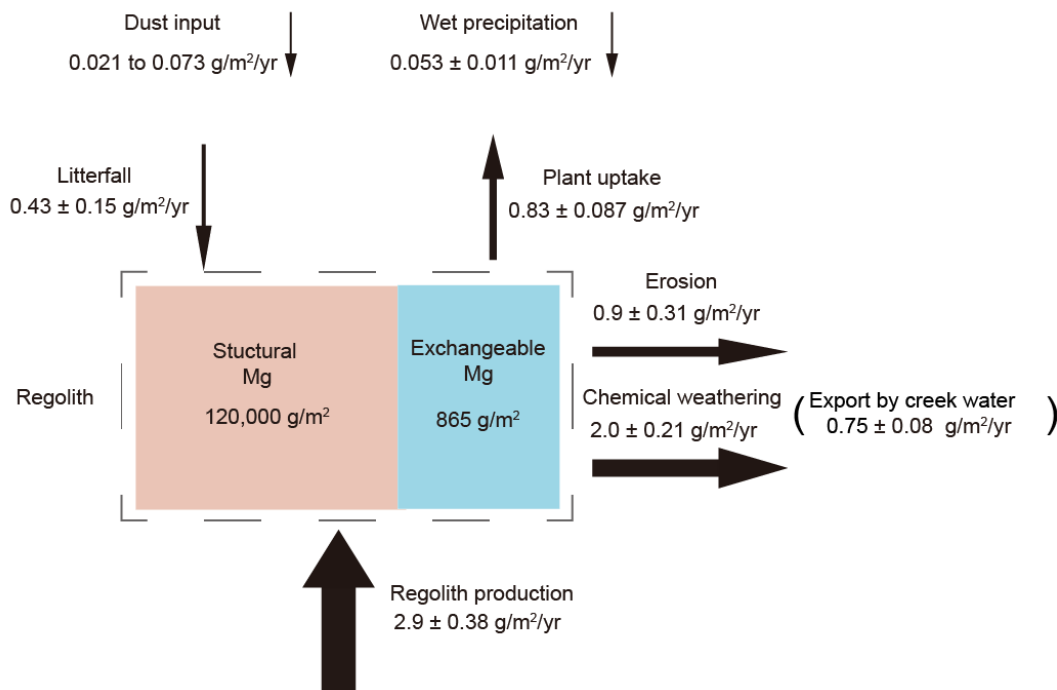
100

101 To fill gaps in the understanding of Mg isotope fractionation during weathering processes, we
102 conducted a comprehensive study in a small, forested catchment underlain by felsic metamorphic
103 rock (Conventwald, Black Forest, Germany). Along with measurements of the Mg isotope
104 composition of bedrock, bulk regolith, clay-sized fraction, and exchangeable fraction of regolith,
105 we investigated the potential controlling factors on the Mg isotope composition of water. We
106 collected time series samples of not only stream water but also groundwater and subsurface flow
107 from 0-15 cm and 15-150 cm below the surface. We suggest that the vertical distribution of the Mg
108 isotope composition of the exchangeable fraction is due to weathering imprinted by biological
109 cycling. Exchange reactions in our catchment are a primary control on water chemistry as $\delta^{26}\text{Mg}$
110 values of water are like those of the exchangeable fraction at depths where it was collected. To
111 further interrogate this finding, adsorption and desorption batch experiments using soil samples
112 from our study site were carried out, indicating negligible fractionation during exchange processes.
113 This combination of field research and lab experiments informs about processes fractionating Mg
114 in the critical zone and further verifies the potential of Mg isotopes as a tool in tracing continental
115 weathering process.

116 **2. Geological setting**

117 Samples were collected from an instrumented forest “Conventwald” (48°02'0N, 7°96'0E), located
118 in the Black Forest, southern Germany. This study site is part of the long-term forest ecosystem
119 monitoring program “International Co-operative Program on assessment and monitoring of air
120 pollution effects on forests (ICP Forest Level II)” and represents also one of the study sites of the
121 DFG priority program SPP 1685 “Ecosystem Nutrition—Forest Strategies for limited Phosphorus
122 Resources”. The monitored creek catchment has an area of 0.077 km² and the average elevation
123 was ~840 m.a.s.l.. Mean annual temperature of the study site was 6.8 °C, and mean annual
124 precipitation was 1395 mm/yr. The underlying bedrock is paragneiss, which was developed from
125 metamorphosed sedimentary rock in the Precambrian. Weathered bedrock was found at ~7 m depth
126 and unweathered bedrock was encountered at ~16 m depth during a core-drilling campaign. The
127 main Mg-hosting minerals in the bedrock include hornblende, chlorite, biotite. Based on
128 microscopic investigations, chlorite and biotite were formed from metamorphosed hornblende. The
129 soil type is a hyperdystric skeletal folic Cambisol with a loamy or sandy loamy texture and a mor-

130 type moder forest floor atop. A detailed description is provided by Lang et al. (2017). The study
 131 site was not glaciated during the Quaternary. Periglacial slope deposits developed during the last
 132 glacial maximum. The uppermost meter of soil had a rock fragment content of ~70%. The
 133 vegetation is mainly composed of European beech (*Fagus sylvatica*, ~40%) and Norway spruce
 134 (*Picea abies*, ~45%). Previous element budget calculations for this site were presented by Uhlig
 135 and von Blanckenburg, (2019). The result for Mg is shown in Fig. 1 for reference.



136
 137 **Fig. 1** Input-output Mg budget of this catchment. Data from Uhlig and von Blanckenburg (2019)
 138 and Uhlig et al. (2020). Arrow width corresponds to the flux magnitude. The chemical weathering
 139 Mg flux is calculated from the total denudation rate, the Mg concentration in unweathered bedrock
 140 and the Mg loss in regolith (τ_{Zr}^{Mg} , section 4.1). The export by creek water Mg flux is calculated from
 141 creek discharge and Mg concentrations in creek water.

142

143 3. Methods

144 3.1. Sampling

145 The sampling strategy was presented in detail by Uhlig and von Blanckenburg (2019) for regolith
 146 samples and Sohr et al. (2019) for water samples. Briefly, shallow regolith was sampled at depth

147 increments of 20 cm in a 3 m deep trench. Deeper regolith beyond 3 m was retrieved using diesel-
148 powered wireline core-drilling to ~20 m. Time series water samples were collected from
149 01.03.2015 to 25.02.2016. Open rainfall and throughfall were collected biweekly in bulk container
150 coved by a netting mesh. Creek discharge and groundwater were collected daily at midnight by
151 autosampler. The groundwater table level was monitored by a pressure probe installed 8.5 m below
152 the surface. Subsurface flow from subsurface flow collectors (see Bachmain and Weiler 2012) was
153 collected at three depths intervals: 0-15 cm, 15-150 cm, and 150-320 cm. Due to limited availability
154 of water samples from 150-320 cm subsurface flow, we only analyzed the other two shallow
155 subsurface flow samples in this study. All the water samples were acidified and stored at 4 °C before
156 analysis. Living wood, beech leaves and spruce needles were collected from representative mature
157 and young trees. Roots are not considered in our study due to the difficulties in root sampling whilst
158 preserving the integrity of trees and the chemical pre-treatment required for isotope analysis.

159

160 **3.2. Extraction of the exchangeable fraction, separation of the clay-** 161 **sized fraction and primary minerals**

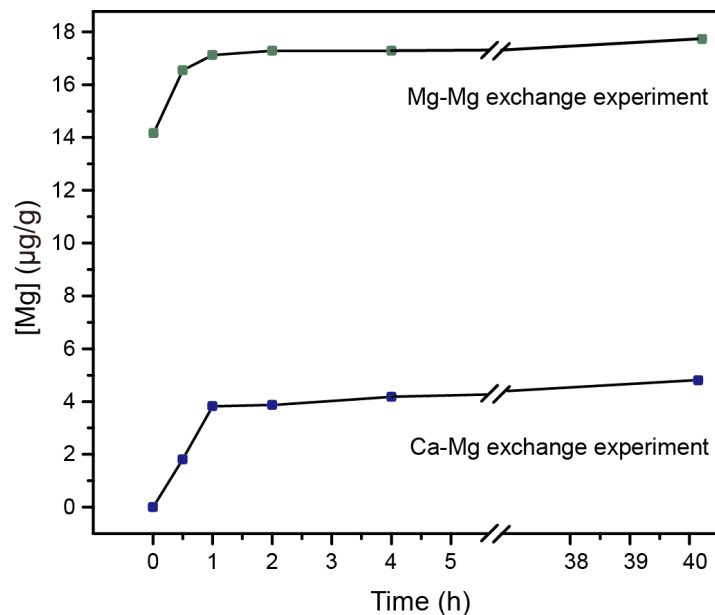
162 Soil and saprolite samples were first oven-dried and sieved to < 2 mm. Two grams of the selected
163 samples were accurately weighed and added to 15 ml acid-cleaned polypropylene centrifuge tubes
164 pre-filled with 14 ml of a 1M NH₄OAc solution. Samples were agitated, and the resulting
165 suspensions shaken on a hotdog roller at 60 rpm for 3 hours. After reaction, the suspensions were
166 centrifuged at 4200 rpm for 30 min, before the supernatant was pipetted off into a syringe and
167 filtered through a 0.2 µm acetate filter. Solutions were then split into two separate aliquots for major
168 element concentration and Mg isotope analysis. Afterward, the NH₄OAc-extracted soil and
169 saprolite samples were twice rinsed with Milli-Q water. The clay-sized fractions of these samples
170 were then extracted by centrifugation following the USGS method (Poppe et al., 2012). To evaluate
171 the Mg isotope composition of different minerals in bedrock, the main Mg-hosting minerals were
172 separated. Bedrock was first crushed and then sieved to 125 µm - 1 mm. The felsic minerals (mainly
173 quartz, and feldspar in this study) were first removed using a magnet separator. Hornblende,
174 chlorite, and biotite were hand-picked under a microscope. Chlorite and biotite grains, formed from
175 metamorphosed hornblende, generally contained trace relicts of hornblende.

176

177 **3.3. Mg isotopes adsorption-desorption experiment using topsoil**

178 To investigate whether Mg isotopes fractionate during adsorption and desorption, we conducted a
179 series of batch experiments using topsoil collected at 5 cm depth from our study site. Prior to the

180 batch experiments, the exchange kinetics of Mg on the soil surface was investigated, to determine
181 the reaction time required to reach equilibrium. Two aliquots of 3 g untreated soil samples were
182 soaked in 30 ml pH-neutral CaCl_2 (30 $\mu\text{g/g}$) and MgCl_2 (14 $\mu\text{g/g}$) solutions, respectively. During
183 reaction, 0.5 ml aliquots of solution were pipetted out after 0.5 h, 1 h, 2 h, 4 h and 40 h for Mg
184 concentration measurements. The results of this preliminary experiment indicate that the exchange
185 reaction was rapid, with near-equilibrium reached within 2 - 4 hours (Fig. 2). In the following
186 experiment, soils were reacted with solution for 3 hours: long enough to reach near equilibrium,
187 but not too long so as to avoid potential dissolution of structural Mg in the soil. In the Mg desorption
188 experiment, circumneutral Milli-Q water (pH 6.2), acidified Milli-Q water (pH 3.2) and CaCl_2
189 solutions of different concentration and pH were reacted with untreated soil to desorb exchangeable
190 Mg. After reaction for 3 hours, the suspensions were centrifuged, before the supernatant was
191 pipetted off into a syringe and filtered from remaining solids for major element concentration and
192 Mg isotope analysis. Procedures for the Mg adsorption experiment were largely identical to those
193 of the Mg desorption experiment, except that MgCl_2 solutions were used instead of CaCl_2 solutions.
194 Similarly, untreated soil samples were immersed in neutral MgCl_2 solutions ([Mg] of 0.6 to 61
195 $\mu\text{g/g}$) or acidic MgCl_2 solutions ([Mg] of 0.6 to 19 $\mu\text{g/g}$). A detailed description of experimental
196 procedures can be found in the Supplementary Material and the associated data publication (Cai et
197 al. 2021).
198



199 **Fig. 2** Kinetics of Mg exchange demonstrated by the magnesium concentration ([Mg]) over time
200 in filtered aliquots of soil suspension solution (see text for details). In both our Ca-Mg and Mg-Mg
201 exchange experiments, near-equilibrium was reached in 2 - 4 hours.

202 **3.4. Instrumental methods**

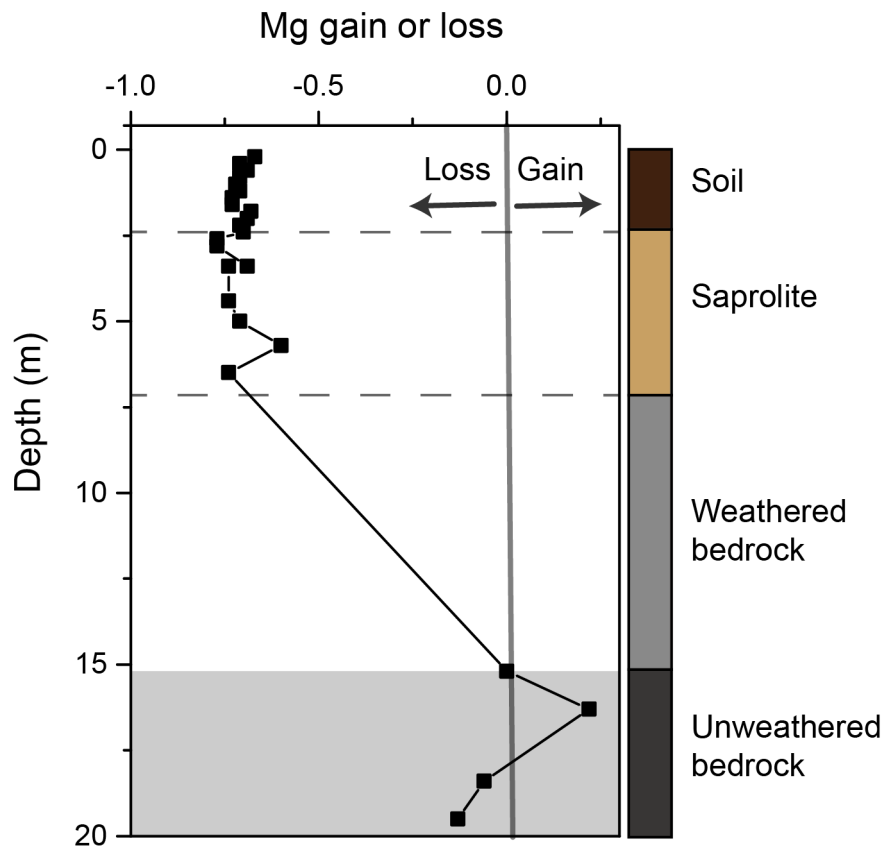
203 All measurements were performed in the Helmholtz Laboratory for the Geochemistry of the Earth
204 Surface (HELGES) at GFZ Potsdam. Soil, saprolite, the extracted clay-sized fraction, primary
205 minerals, and bedrock were dissolved by acid digestion using a mixture of concentrated HF and
206 HNO₃ in PFA vials. Aqua regia was also applied to assist digestion after HF and HNO₃ treatment.
207 Elemental concentrations of the filtered supernatant, water samples, and acid digested solution were
208 analyzed by inductively coupled plasma optical emission spectrometry (ICP-OES, Varian 720-ES)
209 following published protocols (Schuessler et al., 2016). Relative uncertainties are better than 5%
210 for Mg based on repeat analyses of the international reference materials SLRS-6 (river water, NRC
211 CNRC), SRM2709a (soil, USGS) and synthetic in-house standards. The chromatography procedure
212 for Mg purification is described in detail in the Supplementary Material and is the same as that used
213 in Uhlig et al. (2017). Magnesium isotopes were measured via multicollector inductively coupled
214 plasma mass spectrometry (MC-ICP-MS, Thermo Scientific Neptune) using DSM3 as bracketing
215 standard to correct for instrumental mass bias (Galy et al., 2003). Analytical results are reported
216 relative to DSM3 in delta notation, $\delta^x\text{Mg}_{\text{sample}} = [(^x\text{Mg}/^{24}\text{Mg})_{\text{sample}} / (^x\text{Mg}/^{24}\text{Mg})_{\text{DSM3}} - 1] \times 10^3$,
217 where x = 26 or 25. Reference materials Cambridge-1 (pure Mg solution), SLRS-6 (river water),
218 SRM2709a (soil), SRM1515 (apple leaves) are routinely monitored, yielding values of $-2.60 \pm 0.07\text{‰}$
219 (n=24), $-1.24 \pm 0.14\text{‰}$ (n=11), $-0.16 \pm 0.04\text{‰}$ (n=8), $-1.20 \pm 0.04\text{‰}$ (n=3) respectively, which
220 agree well with previously published values (e.g. Shalev et al., 2018).

221 **4. Results**

222 **4.1. $\delta^{26}\text{Mg}$ values in primary minerals, bulk regolith clay-sized fraction, 223 and the exchangeable fraction**

224 Primary Mg-bearing minerals include hornblende, biotite, and chlorite. Both biotite ($-0.08 \pm 0.05\text{‰}$)
225 and chlorite ($-0.13 \pm 0.09\text{‰}$) are slightly enriched in heavy Mg isotopes compared to hornblende
226 ($-0.21 \pm 0.05\text{‰}$). However, reported $\delta^{26}\text{Mg}$ values of biotite, chlorite and hornblende fall within
227 the range found in earlier studies (e.g. Tipper et al. 2006b, 2012; Ryu et al. 2011, 2016; Chapela-
228 Lara et al. 2017). Other silicate minerals (mainly feldspar and quartz) containing relatively little
229 Mg (contributing less than 10% of total Mg in bedrock) exhibit significantly more negative $\delta^{26}\text{Mg}$

230 values ($-0.42 \pm 0.07\text{‰}$). Bulk bedrock shows a similar Mg isotope composition to hornblende,
 231 consistent with being the major host phase of Mg.
 232 The $\delta^{26}\text{Mg}$ values of soil and saprolite show little variation and are on average 0.2‰ more positive
 233 than bedrock. $\tau_{\text{Zr}}^{\text{Mg}}$, calculated as $\frac{[\text{Mg}]_{\text{sample}}/[\text{Zr}]_{\text{sample}}}{[\text{Mg}]_{\text{bedrock}}/[\text{Zr}]_{\text{bedrock}}} - 1$ (Brimhall and Dietrich, 1987), using Zr
 234 as the reference element as justified in Uhlig and von Blanckenburg (2019), suggests $\sim 70\%$ loss
 235 of Mg in the regolith (Fig. 3).
 236 The $\delta^{26}\text{Mg}$ values of the clay-sized fraction is $\sim 0.1\text{‰}$ more positive than bulk regolith from which
 237 it was separated (Fig. 4). Meanwhile, the exchangeable fraction of the regolith exhibits systematic
 238 variation throughout the profile: a decreasing trend in $\delta^{26}\text{Mg}$ values with depth is observed from 0-
 239 1.5 m depth, followed by an increasing trend to -0.52‰ to ~ 3 m, and below 3 m depth values are
 240 largely invariant (Fig. 4). The cation exchange capacity (CEC) of bulk regolith ranges from 0.6 to
 241 8.3 meq/100g (Table S-4). The Mg concentration of the exchangeable fraction relative to the Mg
 242 concentration of bulk soil amounts to $<0.1\%$ and is thus a negligible contribution to the $\delta^{26}\text{Mg}$
 243 values of bulk soil.

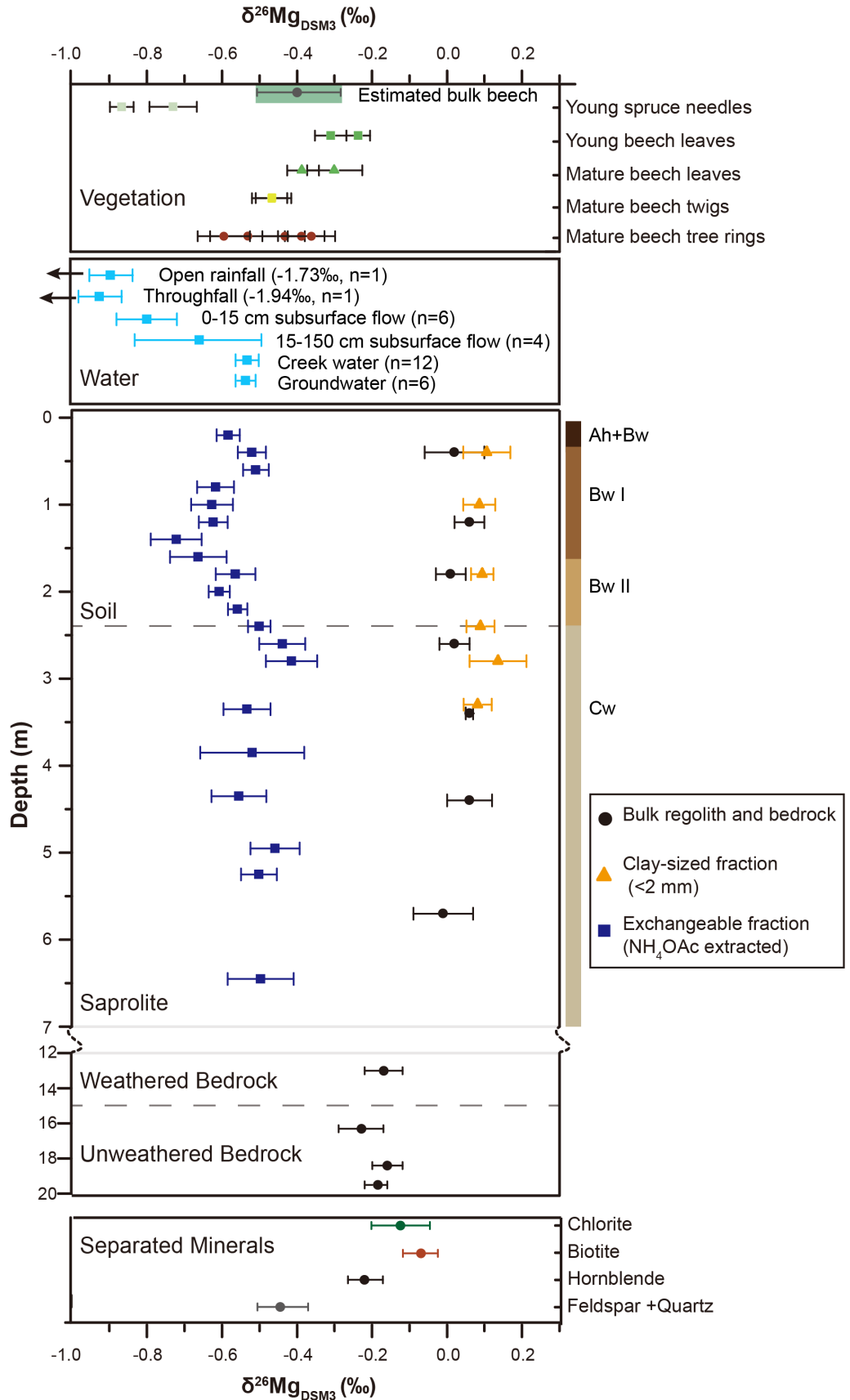


244

245 **Fig. 3** Depth distribution of Mg gain (positive τ_{Zr}^{Mg} values) or loss (negative τ_{Zr}^{Mg} values) in
246 regolith.
247

248 **4.2. $\delta^{26}Mg$ values of plant samples**

249 Plant samples show variable $\delta^{26}Mg$ values among species and tissue types (Fig. 4). Beech tree ring
250 samples span a wide range of $\delta^{26}Mg$ values from -0.61‰ to -0.39‰ with an average of -0.49 ±
251 0.16‰ (mean ± 2SD, n=5). Twigs and leaves are generally more enriched in heavy Mg isotopes
252 than the trunk. Based on Mg allocation in beech tree tissues (4%, 10%, 69% and 17% for foliage,
253 branch, trunk, and roots, respectively, Feger, 1997), the estimated $\delta^{26}Mg$ value of bulk aboveground
254 beech tree is -0.41 ± 0.12‰. Roots were not sampled in this study. To estimate their composition,
255 an apparent Mg isotope fractionation factor for translocation of Mg from tree roots to trunk
256 ($\Delta^{26}Mg_{root-trunk}$) was compiled from previous field studies for sugar maple (Kimmig et al. 2018) and
257 Norway spruce (Bolou-Bi et al. 2012, Novak et al. 2020a,b) and amounts to 0.31 ± 0.38 ‰ (mean
258 ± 2SD, n=6). The estimated $\delta^{26}Mg$ value of root is thus ~ -0.11 ‰, and bulk whole beech is ~-
259 0.42 ‰, a value indistinguishable from bulk aboveground beech. Spruce needles (-0.74‰ to -
260 0.87‰) are slightly depleted in ^{26}Mg compared to the trunk and exchangeable Mg. This value is
261 similar to the data reported for needles in a Vosges Mountains Forest (Bolou-Bi et al., 2012) and is
262 amongst the most negative $\delta^{26}Mg$ value compiled for biological samples by Pokharel et al. (2018).



264

265 **Fig. 4** Magnesium isotope composition ($\delta^{26}\text{Mg}_{\text{DSM3}}$) of bulk regolith, separated minerals, clay-sized
266 fraction, exchangeable fraction, water samples and plant samples.
267 Ah, Bw, Cw: Soil horizons according to IUSS/ISRIC/FAO 2006. For water samples, error bars
268 represent 2SD of the mean value of time series samples. For other samples, error bars represent
269 2SD of four replicate measurements (similarly hereinafter).

270

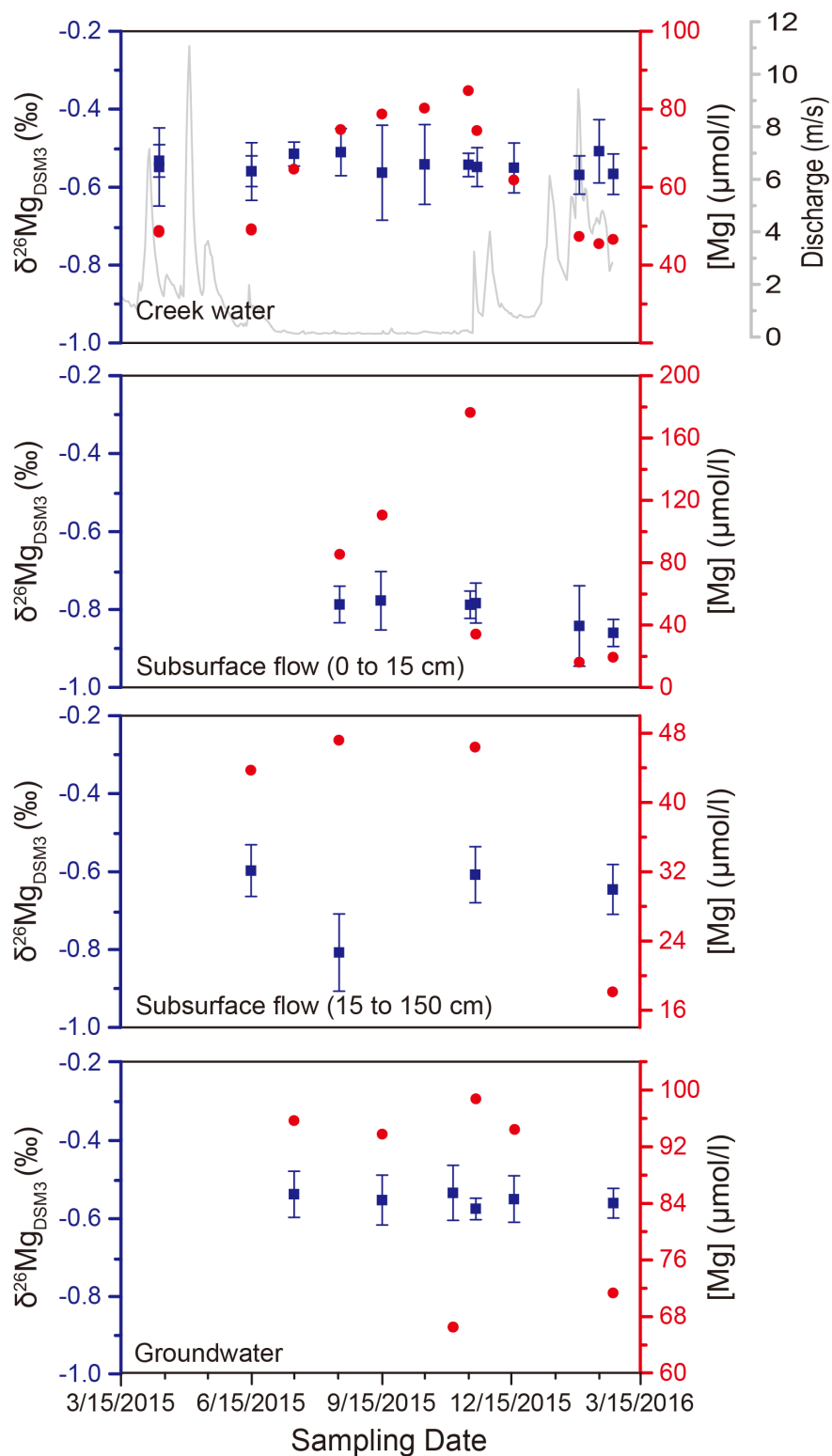
271 **4.3. Mg concentration and $\delta^{26}\text{Mg}$ values of time series water samples**

272 Subsurface water flow collected from 0-15 cm depth show the largest variation in Mg concentration
273 ([Mg]) among all water samples, ranging from 17 to 184 $\mu\text{mol/l}$, which is expected due to dilution
274 with open rainfall or condensation through evaporation. $\delta^{26}\text{Mg}$ values, however, show little
275 variation ($-0.80 \pm 0.08\text{‰}$ mean \pm 2SD, $n=6$) across different seasons and hydrological conditions.
276 Despite the shallow depth at which the subsurface flow was collected, these $\delta^{26}\text{Mg}$ values are
277 significantly more positive than the open rainfall ($-1.73 \pm 0.03\text{‰}$) and throughfall ($-1.97 \pm 0.03\text{‰}$).
278 Similarly negative $\delta^{26}\text{Mg}$ values of open rainfall were also observed in the Damma glacier
279 catchment in Switzerland (-1.29 to -1.59‰ , Tipper et al., 2012) and the Hermine Experimental
280 Watershed in Canada (-1.58 to -2.22‰ , Kimmig et al., 2018). The negative $\delta^{26}\text{Mg}$ values of open
281 rainfall may result from the dissolution of carbonate dust in rain (Tipper et al., 2012; Kimmig et al.,
282 2018). The lighter Mg isotopes in throughfall may reflect the leaching of isotopically light Mg
283 from the canopy such as the unbonded Mg contained in cells that is depleted in ^{26}Mg as compared
284 to Mg in Chlorophyll or other bonded Mg forms (Kimmig et al., 2018; Pokharel et al., 2018).
285 Subsurface flow collected from 15-150 cm depth shows relatively smaller [Mg] variation, ranging
286 from 19 to 49 $\mu\text{mol/l}$ and on average, Mg concentrations are lower than for the 0-15 cm depth
287 section. Except for one subsurface flow sample from 15-150 cm depth collected in August, which
288 has identical $\delta^{26}\text{Mg}$ values ($-0.84 \pm 0.03\text{‰}$) to that collected from the 0-15 cm depth section,
289 subsurface flow samples collected from 15-150 cm depth show consistently more positive $\delta^{26}\text{Mg}$
290 values than their shallower counterparts ($-0.62 \pm 0.04\text{‰}$, $n=3$).

291

292 Groundwater [Mg] is generally twice as high in concentration as 15-150 cm subsurface flow, and
293 ranges between 65 and 99 $\mu\text{mol/l}$. Despite changing [Mg], $\delta^{26}\text{Mg}$ values of groundwater remain
294 invariant ($-0.55 \pm 0.03\text{‰}$, $n=6$). However, although discharge variations span two orders of
295 magnitude, [Mg] at low flow is only twice as high than [Mg] during high flow periods. Intriguingly,
296 despite the large variability in discharge and the minor variability in [Mg] over the sampling period,

297 no corresponding change in the $\delta^{26}\text{Mg}$ value of creek water was observed ($-0.54 \pm 0.04\text{‰}$, $n=12$),
298 with values remaining identical to that of groundwater.
299



300

301 **Fig. 5** Magnesium isotope composition ($\delta^{26}\text{Mg}_{\text{DSM3}}$, left axis) and Mg concentration ($[\text{Mg}]$, right
302 axis) of time-series water samples including creek water, subsurface flow and groundwater sampled
303 from a well at 8 m depth. The grey curve in the background of the uppermost panel shows the creek
304 discharge.

305

306 **4.4. Adsorption and desorption experiment on topsoil**

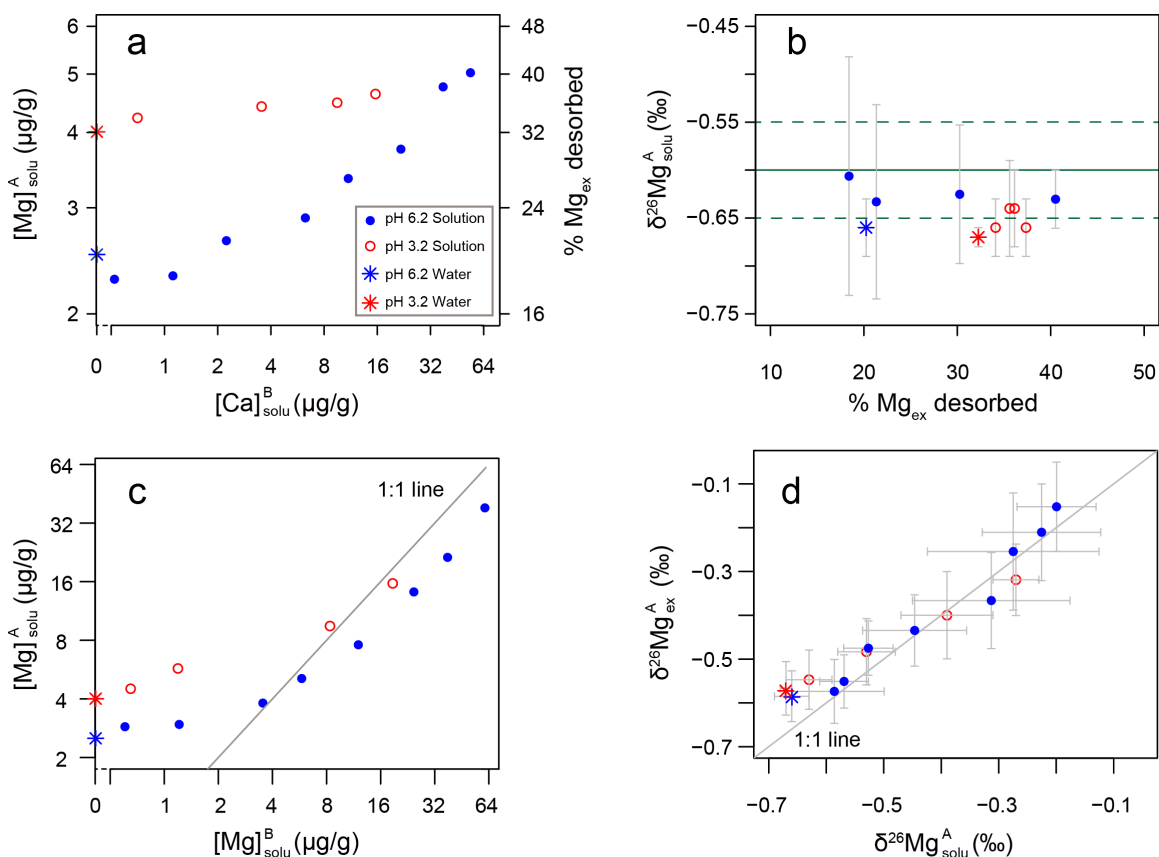
307 **4.4.1. Mg desorption experiment**

308 Assuming excess NH_4OAc could extract all the exchangeable Mg from soil, we found that 20% of
309 Mg was desorbed with circumneutral Milli-Q water (pH 6.2) and 32% was desorbed with Milli-Q
310 acidified to pH 3.2 with a few drops of distilled HNO_3 . In both acidic and circumneutral conditions,
311 increasing $[\text{Ca}]$ in solution could exchange more Mg, although the increase in Mg desorbed with
312 higher Ca input is considerably weaker at low pH compared to circumneutral pH (Fig. 6a).
313 Importantly, however, despite the difference in the amount of Mg desorbed, the $\delta^{26}\text{Mg}$ value of all
314 reacted solutions remain almost identical or slightly more negative ($< 0.1\%$) than that of bulk soil
315 exchangeable Mg (Fig 6b), suggesting the exchangeable Mg was congruently released to the
316 solutions with little or no fractionation.

317

318 **4.4.2. Mg adsorption experiment**

319 Patterns of Mg adsorption (and desorption) equilibrium after soil was reacted with MgCl_2 solutions
320 are shown in Fig. 6. Data points above the 1:1 line indicate increasing $[\text{Mg}]_{\text{solu}}$ after reaction, thus
321 a net desorption, while those below the 1:1 line suggest net adsorption during the experiment (Fig.
322 6c). This result suggests that desorption and adsorption on natural soil depends on both solution pH
323 and input solution Mg concentration. After reaction, regardless of whether adsorption or desorption
324 was dominant, exchangeable Mg had $\delta^{26}\text{Mg}$ values that were almost identical to solution Mg (Fig.
325 6d), suggesting that isotope fractionation is negligible.



327 **Fig. 6** Results of adsorption-desorption experiments. **Panel a)** depicts the influence of the calcium
 328 concentration in the solution ($[Ca]$) on the amount of desorbed Mg. $[Ca]_{solu}^B$ denotes Ca
 329 concentration in the solution before reaction. $[Mg]_{solu}^A$ denotes the Mg concentration in the solution
 330 after reaction. The right-hand y-axis shows the percentage of total exchangeable Mg that is
 331 desorbed. Both axes are in log scale. The star symbols denote circumneutral or pH 3.2 water. **Panel**
 332 **b)** shows the relationship between the proportion of Mg desorbed and the isotope composition of
 333 desorbed Mg ($\delta^{26}Mg_{solu}^A$). Horizontal solid and dashed lines represent the $\delta^{26}Mg$ value and its
 334 analytical uncertainty (2SD) of the exchangeable fraction of the sample used for the desorption
 335 experiment. The data suggests that Mg was released with no or little fractionation. **Panel c)** Mg
 336 concentrations in solutions before ($[Mg]_{solu}^B$, x-axis) and after ($[Mg]_{solu}^A$, y-axis) reaction
 337 respectively. Data points above the 1:1 line imply desorption while points below the line imply
 338 adsorption. Both axes are in log scale. **Panel d)** Mg isotope composition of solution ($\delta^{26}Mg_{solu}^A$)
 339 and absorbed fraction ($\delta^{26}Mg_{ex}^A$) after reaction. The data points are generally distributed along the
 340 1:1 line, indicating negligible fractionation between solution Mg and exchangeable Mg after
 341 reaction.

342

343 **5. Discussion**

344 **5.1. The absence of isotope fractionation during adsorption-desorption** 345 **experiments**

346 Our lab experiments suggest that soil exchangeable Mg is congruently desorbed to solution without
347 isotope fractionation, regardless of pH, solution chemistry or proportion of Mg released. Similarly,
348 no or very small (<0.1‰) fractionation was observed in Mg adsorption experiments, even though
349 pH exerted a strong influence on the adsorption-desorption equilibrium. We infer that Mg
350 adsorption is non-specific in the sense that it does not involve changes in inner-sphere complexation.
351 The rationale is as follows: if Mg were adsorbed as an inner-sphere complex, then isotopic
352 fractionation might be expected during the process of dehydration and formation of covalent bonds.
353 For example, molecular dynamics simulations of Mg isotope fractionation amongst aqueous Mg
354 species predict fractionations in the range of one to several per mil (Schott et al., 2016). In this case,
355 hydrated Mg, typically represented as $\text{Mg}[\text{H}_2\text{O}]_6^{2+}$ in molecular dynamics simulations (Trivedi and
356 Axe, 2001), is electrostatically attracted to the surface without undergoing dehydration and forming
357 chemical bonds, and thus no isotope fractionation occurs. That Mg is readily exchanged by Ca
358 lends support to this interpretation. In line with Charlet and Sposito (1989), our study showed that
359 Mg adsorption is depressed when solution electrolyte concentration increases, a characteristic of
360 non-specific sorption mechanism.

361

362 **5.2. Mg isotope fractionation in regolith: preferential dissolution and** 363 **secondary mineral formation**

364 In the upper ~7 m the $\delta^{26}\text{Mg}$ value of bulk regolith (soil and saprolite) is ~ 0.03‰, a value in
365 between that of the remaining primary minerals (biotite and chlorite) and the clay-sized fraction
366 (Fig. 4), and on average 0.2‰ more positive than bedrock. In previous field studies, secondary
367 mineral formation has been widely assumed to be the main factor fractionating Mg isotopes in soil
368 (e.g., Teng et al., 2010; Liu et al., 2014). However, we observed that minerals separated from
369 bedrock are heterogeneous in their Mg isotope composition. Among the main Mg-bearing minerals,
370 biotite and chlorite are more enriched in ^{26}Mg than hornblende. Thus, differential dissolution of
371 primary minerals might cause the observed depletion in ^{24}Mg in regolith. Indeed, X-ray diffraction
372 analyses suggests that hornblende, the Mg phase with a low $\delta^{26}\text{Mg}$ value (-0.21‰) is abundant in

373 the bedrock but undetectable in the upper 7 m of regolith (Uhlig and von Blanckenburg, 2019),
374 suggesting it has been dissolved due to its higher solubility. Therefore, the more positive Mg
375 isotope composition we observed in soil and saprolite might be due to dissolution of hornblende.
376 However, biotite (-0.13‰) and chlorite (-0.08‰), the remaining two Mg carriers, are still by ~0.1‰
377 isotopically lighter than the bulk soil and saprolite ($0.03 \pm 0.06‰$, n=6). We thus explore next
378 whether secondary mineral formation causes the difference in the Mg isotope composition between
379 bedrock and regolith.

380

381 The clay-sized fraction was extracted from regolith and yields a $\delta^{26}\text{Mg}$ value of $0.10 \pm 0.04‰$ (n=6),
382 a value more positive than bulk regolith and separated minerals. Because the clay-sized fraction is
383 composed of truly neoformed secondary minerals and fine primary minerals, the $\delta^{26}\text{Mg}$ values of
384 the secondary minerals are assumed to be even more positive than the mixture. An upper
385 approximation of the relative amount of neoformed secondary minerals can be estimated by a
386 simple mass balance (equation 1).

387

$$388 \delta^{26}\text{Mg}_{\text{soil}} = (1 - f_{\text{secondary}}) \times \delta^{26}\text{Mg}_{\text{primary}} + f_{\text{secondary}} \times \delta^{26}\text{Mg}_{\text{secondary}} \quad (1)$$

389

390 In equation 1 $\delta^{26}\text{Mg}_{\text{primary}}$ represents the mean $\delta^{26}\text{Mg}$ value of biotite and chlorite (-0.11‰),
391 $\delta^{26}\text{Mg}_{\text{secondary}}$ is the most positive $\delta^{26}\text{Mg}$ value of our separated clay-sized fraction (0.12‰), and
392 $f_{\text{secondary}}$ is the relative proportion of neoformed secondary minerals. Given that $f_{\text{secondary}}$
393 amounts to ~52%, half of the soil Mg is hosted in secondary minerals. The incorporation of heavy
394 Mg isotopes into clays is also supported by the low $\delta^{26}\text{Mg}$ value in the remaining fluid (e.g.,
395 subsurface flow water) and the exchangeable fraction; a topic we return to section 5.3.2.

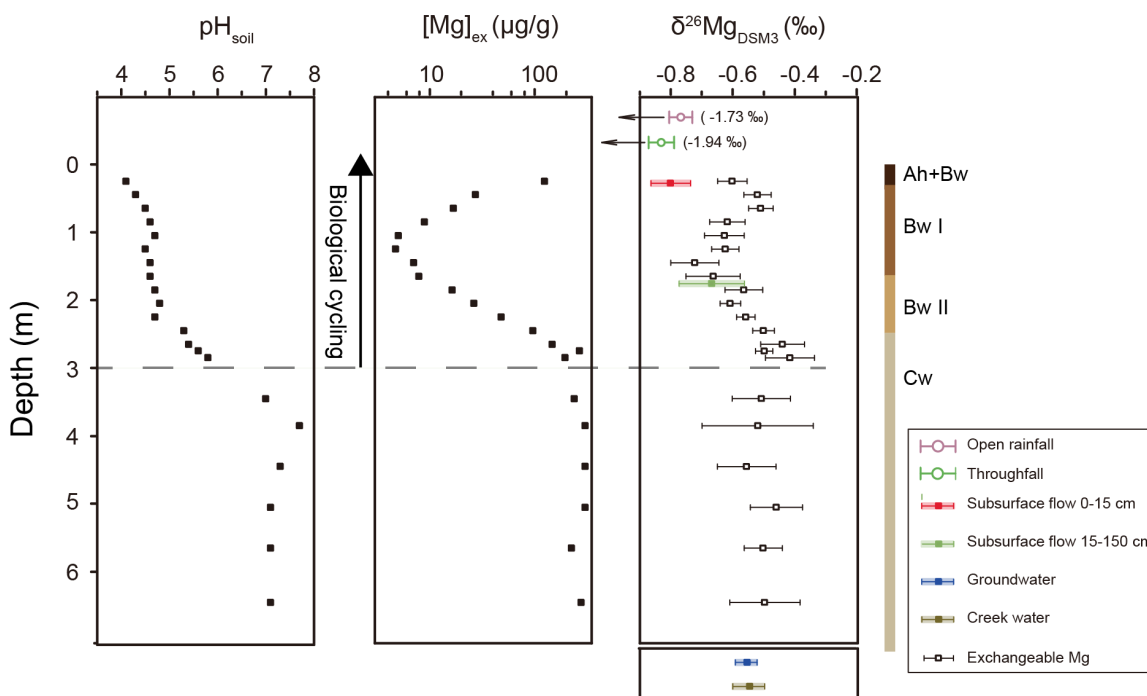
396 In summary, we suggest that the positive $\delta^{26}\text{Mg}$ value of the regolith is due to a combination of 1)
397 dissolution of isotopically light hornblende and 2) secondary mineral formation further
398 fractionating Mg isotope in regolith towards more positive $\delta^{26}\text{Mg}$ values.

399

400 **5.3. Source and vertical distribution of isotopically light exchangeable** 401 **Mg**

402 The vertical distribution of the Mg concentration and Mg isotope composition of the exchangeable
403 fraction can be divided into two parts: from 0 to 3 m, showing a bulge pattern with low Mg
404 concentrations and more negative $\delta^{26}\text{Mg}$ values in the center of the bulge; and from below 3 m
405 depth, where Mg concentration and $\delta^{26}\text{Mg}$ values of the exchangeable fraction are almost invariant

406 (Fig. 7), a pattern similar to that found by Kimmig et al., (2018). Whereas the vertical distribution
 407 of element concentrations in the exchangeable fraction has been explained in previous studies
 408 through supply from atmospheric deposition, dissolution of primary minerals, and biological
 409 cycling (Jobbágy and Jackson, 2001; James et al., 2016; Uhlig and von Blanckenburg, 2019; Yu et
 410 al., 2020), the depth distribution of the Mg isotope composition remains poorly constrained.
 411



412 Fig. 7 Vertical distribution of soil pH (pH_{soil}), Mg concentration ($[\text{Mg}]_{\text{ex}}$) and Mg isotope
 413 composition ($\delta^{26}\text{Mg}_{\text{DSM3}}$) of the exchangeable fraction (1M NH_4OAc). The bulged distribution of
 414 $[\text{Mg}]_{\text{ex}}$ and $\delta^{26}\text{Mg}$ values in shallow soil (0 – 3 m) is attributed to chemical weathering imprinted
 415 by biological cycling, which increases from 3 m depth (dashed line) to the top of the soil profile
 416 (indicated by the arrow, see text for detail). The $\delta^{26}\text{Mg}$ values of water samples including open
 417 rainfall (n=1), throughfall (n=1), subsurface flow from 0-15 cm (n=6) and 15-150 cm depth (n=4),
 418 groundwater (n=6), and creek water (n=14) was also shown for comparison.
 419

420 5.3.1. Biological impact on the Mg concentration and isotope composition of the 421 exchangeable fraction at shallow regolith (0 to 3 m)

422 The biological nutrient uplift hypothesis from Jobbágy and Jackson (2001) describes how mineral
 423 nutrients are biologically uplifted and recycled; in other words, plants take up mineral nutrients
 424 from depth and return them to the forest floor via litterfall, from which they can be readily re-
 425 utilized. Consequently, concentrations of mineral nutrients in the exchangeable fraction of soil

426 increase from depth to topsoil. However, previous studies lack direct evidence that elements hosted
427 in the exchangeable fraction of topsoil can be attributed to biological uplift. Our new dataset
428 comprising the paired analyses of Mg concentrations and isotope compositions allows for an
429 assessment of the biological nutrient uplift hypothesis.

430 The depth profile of the Mg concentration of the exchangeable fraction was described earlier in
431 Uhlig and von Blanckenburg (2019). Importantly, the increasing Mg concentration from 1.5 m
432 depth to topsoil was attributed to biological uplift, which agrees with the studies of Jobbágy and
433 Jackson (2001, 2004). In this case, Mg is utilized by trees at depth (1.5 - 3 m) with heavy Mg
434 isotopes being favored, which agrees with results from $^{87}\text{Sr}/^{86}\text{Sr}$ and $^{10}\text{Be}(\text{meteoric})/^{9}\text{Be}$ ratios used
435 as nutrient uptake tracer in Uhlig et al. (2020). The Mg is then cycled through trees and a fraction
436 is ultimately returned to the forest floor via annual litterfall. As Mg is not significantly re-utilized
437 from organic matter in this study site (Uhlig and von Blanckenburg 2019), isotopically heavy Mg
438 liberated from decomposing plant litter or organic matter may re-enter the pool of the exchangeable
439 fraction.

440 In support of this suggested mechanism the increase of both $[\text{Mg}]_{\text{ex}}$ and $\delta^{26}\text{Mg}_{\text{ex}}$ values from 1.5 m
441 to the forest floor is consistent with the observation that beech leaves (representing plant litter) are
442 enriched in heavy Mg isotopes. Even though Uhlig and von Blanckenburg (2019) concluded that
443 trees do not set the stoichiometry of the exchangeable fraction of the upper three meters of soil,
444 their general statement may not hold for elements such as Mg that are not significantly re-utilized.
445 In summary, we conclude that the $\delta^{26}\text{Mg}_{\text{ex}}$ value of the top 3 m of our profile is first set by
446 secondary mineral formation (see below), to be then overprinted by Mg uptake by trees (at 1.5 to
447 3 m depth) and biological uplift of Mg (in the top 1.5 m).

448

449 **5.3.2. Source of isotopically light Mg in the exchangeable fraction of deep regolith (>3 m)**

450 The exchangeable fraction of deep regolith (>3 m) is characterized by high Mg concentrations and
451 low $\delta^{26}\text{Mg}$ values. Previous studies (e.g., Opfergelt et al., 2014; Chapela Lara et al., 2017; Uhlig et
452 al., 2017; Kimmig et al., 2018) also found that the exchangeable fraction is generally isotopically
453 lighter than bulk regolith. Opfergelt et al. (2014) attributed this phenomenon to isotope
454 fractionation during successive adsorption-desorption processes. However, our adsorption-
455 desorption experiment using topsoil from our study site shows negligible isotope fractionation.
456 Therefore, other factors need to be considered. Both open rainfall and throughfall are depleted in
457 isotopically heavy Mg, but this isotope signature is not likely transferred to several meters depth as
458 demonstrated by a labeling experiment with an artificial ^{26}Mg spike (van der Heijden et al., 2013).
459 In addition, the inventory of the exchangeable Mg pool is more than 10^3 times higher than the

460 annual influx of Mg by atmospheric deposition (Fig. 1). Because the chemical weathering flux of
461 Mg exceeds Mg input by open rainfall by about 40 times, the large exchangeable Mg pool is thought
462 to originate from weathering of the regolith rather than from atmospheric input. Felsic minerals
463 (feldspar and quartz) exhibit $\delta^{26}\text{Mg}$ values similar to exchangeable Mg (Fig. 4), but the Mg
464 concentration in these minerals is too low to be a primary Mg source, amounting to less than 10%
465 relative to biotite and chlorite. Moreover, biotite is more soluble than the felsic minerals (e.g., 1.5
466 $\times 10^{-10}$ mol/g/s for biotite compared to 6.6×10^{-11} mol/g/s for plagioclase in a granite dissolution
467 experiment, Ganor et al., 2004). The isotopically light Mg of the exchangeable fraction thus does
468 not originate from the dissolution of felsic minerals. Carbonate minerals are known to have the
469 most negative $\delta^{26}\text{Mg}$ values in environmental samples (Saenger and Wang, 2014), but microscopic
470 and XRD (Uhlig and von Blanckenburg 2019) analyses failed to identify the presence of carbonate
471 minerals at this site. Eliminating these factors, the most likely process driving the Mg isotope
472 composition of the exchangeable fraction to negative $\delta^{26}\text{Mg}$ values is secondary mineral formation
473 as discussed in section 5.2. It is likely that the Mg residue in soil water entered the exchangeable
474 pool after secondary mineral formation. This is evidenced by former clay synthesis experiments
475 (Hindshaw et al., 2020), which showed 17 - 33 % Mg hosted in exchangeable sites compared to
476 Mg in bulk solid.

477 To identify the surfaces providing exchangeable sites in deep (>3 m) regolith (such as organic
478 matter, phyllosilicates, oxides and hydroxides), we combined mineralogical evidence (XRD
479 analyses in Uhlig and von Blanckenburg (2019)) with the cation exchange capacity (CEC, Table
480 S4). CEC of deep regolith ranges from 5.7 to 8.3 meq/100g. Since most primary minerals like
481 quartz and feldspar have negligible exchange capacity, the CEC of minerals providing exchange
482 sites in the deep regolith will exceed 8.3 meq/100g. As humus with a high CEC of >150 meq/100g
483 (Brady and Weil 2008) can be ruled as major exchangeable site host in the deep regolith, and oxides
484 have a low CEC of <10 meq/100g (Brady and Weil 2008), phyllosilicates likely provide the
485 required exchangeable sites. Identified phyllosilicates in large abundance by XRD (Uhlig and von
486 Blanckenburg 2019) and thin section investigation include chlorite and biotite, which indeed have
487 high CEC (10-40 meq/100g, Brady and Weil 2008). Smectites and vermiculites also have high CEC
488 (80-175 meq/100g, Brady and Weil 2008), but could not be distinguished from biotite using XRD
489 analyses on bulk soil. We thus conclude that the light Mg remaining in solution after formation of
490 secondary minerals is adsorbed onto the exchangeable sites of chlorite and biotite.

491

492 **5.4. Exchangeable fraction as first order control on runoff water** 493 **chemistry**

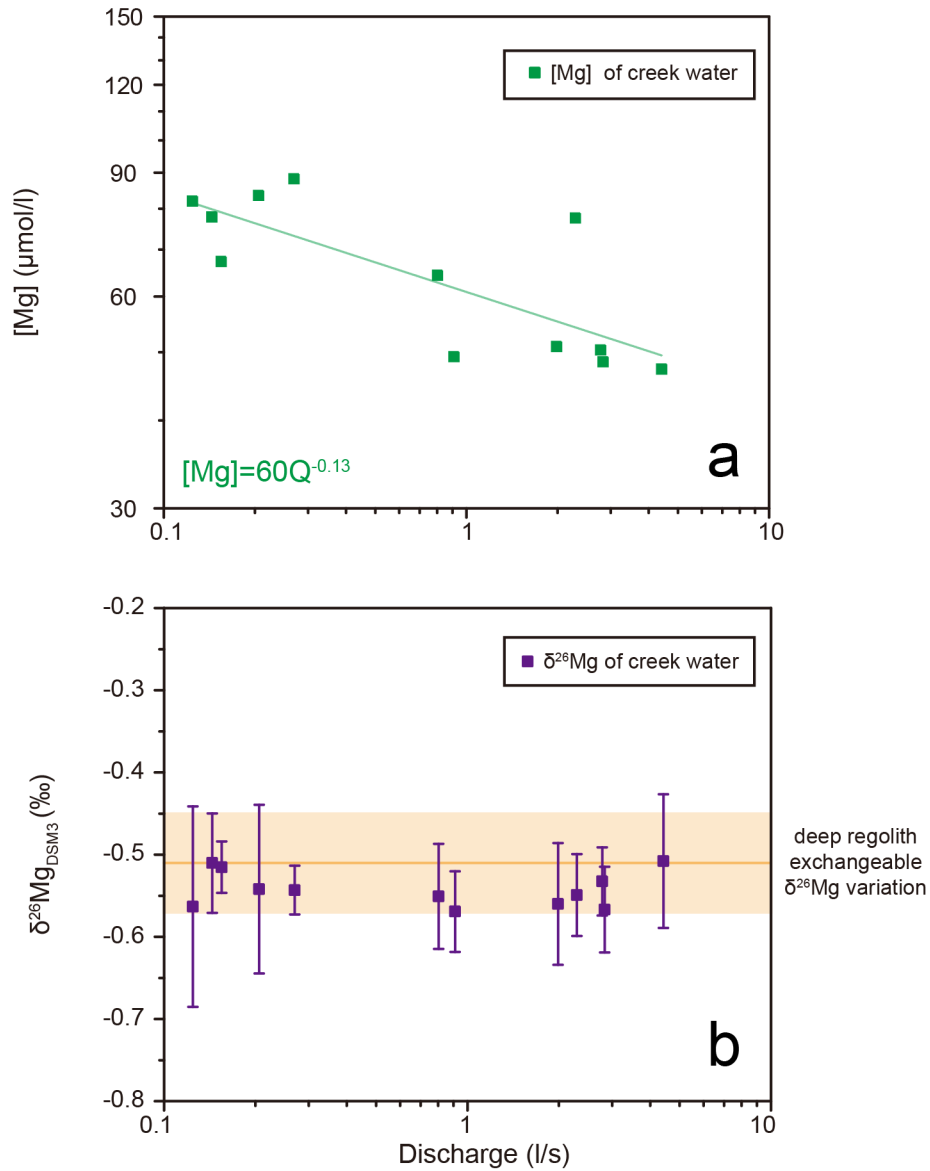
494 It is intriguing that the subsurface flow, groundwater, and creek water show negligible seasonal
495 variation in $\delta^{26}\text{Mg}$ values despite variations in Mg concentration and hydrological condition (Fig.
496 5). More intriguing, $\delta^{26}\text{Mg}$ values of water agree with those of the exchangeable fraction at their
497 respective sampling depth (Fig. 7). For example, groundwater and creek water samples yield almost
498 identical $\delta^{26}\text{Mg}$ values to that of the deep regolith (> 3 m) exchangeable pool, and subsurface flow
499 (15 – 150 cm) samples exhibit uniform $\delta^{26}\text{Mg}$ values that correspond to the value of exchangeable
500 $\delta^{26}\text{Mg}$. As our exchange experiments indicate negligible isotope fractionation during adsorption-
501 desorption (Fig. 6), we hypothesize that the water samples in this study site are in equilibrium with
502 exchangeable pool of corresponding depth. Only in the 0-15 cm subsurface water $\delta^{26}\text{Mg}$ values
503 deviate from the exchangeable pool, being on average $\sim 0.2\%$ more negative (Fig. 7). A potential
504 explanation for this discrepancy is the contribution of throughfall, in which Mg has a very negative
505 $\delta^{26}\text{Mg}$ value. Given the short water flow path length scale of about 15 cm the timescale for
506 desorption may be too low to fully buffer diluted rainwater in terms of concentrations and isotope
507 compositions.

508 Compared to the invariance of the Mg isotope composition in creek water, Mg concentrations
509 dropped by about half when discharge increased by about two orders of magnitude (Fig 8a). This
510 relationship of concentration (C) and discharge (Q) can be described by the power law equation
511 $C=aQ^b$, with a and b being fitted parameters (Godsey et al., 2009). A log-log slope (b-value) of zero
512 represents chemostasis (Godsey et al., 2009) meaning the concentration of a given solute remains
513 constant regardless of discharge, and a b-value of -1 indicates pure dilution behavior. The b-value
514 of -0.13 in this study (Fig.8a) indicates a strong buffering of the Mg concentration, consistent with
515 observations elsewhere (e.g., Godsey et al., 2009; Clow and Mast, 2010; Kim et al., 2017).

516 However, the processes causing this buffering effect on cation concentrations are subject to debate
517 (e.g., Maher, 2010; Trostle et al., 2016; Torres et al., 2017; Kim et al., 2017; Torres and Baronas,
518 2021). What generally missing in previous C-Q studies is direct evidence on the source of Mg
519 supplied to runoff in periods of high water flow. We suggest that it is cation exchange process that
520 buffers Mg concentration in this study site for two reasons. The first reason is the large size of
521 exchangeable Mg in the regolith. Exchangeable Mg hosted in the upper 7 m of regolith lasts for as
522 much as for about 1200 years before being exhausted by solute runoff export into runoff export in
523 this study site (Fig. 1). The second reason is the aforementioned similarity of $\delta^{26}\text{Mg}$ values in
524 dissolved phase and corresponding exchangeable fraction (Fig. 7).When rainwater of low cation

525 concentrations infiltrates into regolith, the water is either initially stored in the vadose zone, or
526 directly recharges groundwater and runoff (e.g. Montgomery and Dietrich 2002; Salve et al., 2012;
527 Sprenger et al, 2016; Kim et al., 2017). This infiltrating water inevitably exchanges cations with
528 the exchangeable pool, which, based on our adsorption-desorption experiments may take place
529 within minutes and reach near-equilibrium in ~ 2 hours (Fig. 2). Soil column leaching experiments
530 have also resulted in significant contributions of exchangeable Mg to the effluent solutions within
531 60 minutes (Oh and Richter Jr. 2004).

532 However, the buffering capacity of the exchangeable pool on infiltrating water reaches a limit
533 during prolonged rainfall events at a so-called “set-point” when dilution effects begin to prevail
534 (Godsey et al. 2019). This limitation is also verified by column leaching experiments showing a
535 decreasing trend of base cations desorbed into leachates at prolonged leaching time (Oh and Richter
536 Jr. 2004; Pogge von Strandmann et al., 2020). As a result, slightly dilution (also buffered compared
537 to pure dilution) effect was seen due to the attenuated exchange reaction. Importantly, even if such
538 dilution prevails, the Mg isotope composition remains unaffected as desorption does not fractionate
539 Mg isotopes (Fig. 6b). When it comes to dry season, Mg concentrations are generally higher in soil
540 water and groundwater due to evaporation and mineral dissolution (caused by longer residence
541 times of water, Maher, 2010; Kim et al., 2014). Therefore, Mg tend to be adsorbed to the
542 exchangeable sites in dry seasons to replenish the exchangeable pool. As such, we propose that the
543 exchangeable pool acts like a buffer regulating Mg concentrations and isotope compositions under
544 a range of hydrological conditions. In support of this hypothesis, we note that our batch Mg
545 adsorption experiments (Fig. 6c) have shown the transition from net desorption to net adsorption
546 with increasing solution Mg concentrations. This explanation may also hold for other studies (e.g.
547 Hindshaw et al., 2019; Fries et al., 2019; Novak et al., 2021) that also showed almost invariant
548 $\delta^{26}\text{Mg}$ values and buffered Mg concentrations in time series runoff samples.



549

550

551 Fig. 8 **a**: Relationship of Mg concentration ([Mg]) with discharge (Q). The Mg concentration is

552 buffered during high flow periods. **b**: Relationship of the Mg isotope composition ($\delta^{26}\text{Mg}$) with

553 discharge of creek water. Horizontal line and shaded area illustrate the mean $\delta^{26}\text{Mg}$ value \pm 2SD of

554 the exchangeable fraction in deep regolith (>3m).

555

556 **5.5. Quantifying dissolved Mg loss by elemental and isotope mass** 557 **balance**

558 In the critical zone, bulk soil integrates the long-term weathering process and water chemistry is
559 the instantaneous weathering product. Using an isotope mass balance approach, Bouchez et al.
560 (2013) developed an isotope model that quantifies the relationship between the weathering flux of
561 the element of interest and the total denudation flux solely by metal isotopes (equation 2).

562

$$563 \quad w^{Mg} = \frac{\delta^{26}Mg_{regolith} - \delta^{26}Mg_{rock}}{\delta^{26}Mg_{regolith} - \delta^{26}Mg_{creek\ water}} \quad (2)$$

564

565 In equation 2, w^{Mg} is the fraction of dissolved Mg export relative to the total export of solute and
566 particulate Mg. $\delta^{26}Mg_{regolith}$, $\delta^{26}Mg_{rock}$, and $\delta^{26}Mg_{creek\ water}$ are the $\delta^{26}Mg$ values of
567 regolith, bedrock and creek water, respectively. The calculated w^{Mg} is $41 \pm 11\%$, indicating that
568 $\sim 41\%$ of total denuded Mg occurs in dissolved form, while the remainder is eroded in particulate
569 form. w^{Mg} can also be evaluated by calculating the relative mass loss of Mg from regolith (τ_{Zr}^{Mg} ,
570 Fig. 4). This method gives a value of $71 \pm 17\%$. The results derived from these two methods are
571 roughly consistent, indicating the robustness of using both methods for evaluation of Mg
572 weathering intensity in the critical zone.

573

574 **6. Conclusion**

575 We hypothesized that the exchangeable fraction exerts the main control on the Mg isotope
576 composition of creek water. Two lines of evidence support this hypothesis: First, results of our
577 laboratory adsorption-desorption experiment show that isotope fractionation during adsorption-
578 desorption processes is negligible and creek water also show $\delta^{26}Mg$ values that are identical to
579 those of the exchangeable fraction in the deep regolith. Second, the pool size of exchangeable Mg
580 suffices over millennia to buffer Mg concentrations in creek water. Thus, the exchangeable fraction
581 of Mg records the Mg isotope composition of the fluid. Moreover, we propose that the pool of
582 exchangeable fraction acts like a buffer regulating water Mg concentrations within a range of
583 hydrological conditions: adsorbing and storing cations in dry seasons, when soil solutions are high
584 in cation concentration, and desorbing cations, when rainwater infiltrates into and percolates
585 through the regolith.

586 We also demonstrate that the vertical distribution of both exchangeable Mg concentration and
587 isotope composition can be reconstructed at high depth resolution in the critical zone. Deep regolith
588 (>3 m) hosts substantial amounts of exchangeable Mg sourced by chemical weathering processes
589 and secondary mineral formation. In contrast, at shallow depth (<3 m) biological cycling
590 significantly overprints the geogenic-impacted Mg isotope composition of the exchangeable
591 fraction through Mg uptake by trees which reaches a depth of up to ~3 m.

592

593 **Acknowledgements**

594 The authors are grateful for funding from the German National Science Foundation Priority
595 Program 1685 “Ecosystem nutrition: forest strategies for limited phosphorus resources” and to
596 Friederike Lang for coordination and discussion. Di Cai is grateful for funding by a CSC
597 scholarship. Johannes Glodny is acknowledged for support on mineral separation. The authors are
598 grateful to the analytical support provided by Jutta Schlegel and Josefine Holtz. Finally, the authors
599 are grateful to the fruitful reviews by Sara Kimmig, two anonymous reviewers and the associate
600 editor Nathalie Vigier that helped to improve the manuscript.

601

602 **Data availability statement**

603 The data set including Tables S1–S6 of this study is accessible in the data repository under the
604 reference Cai et al. 2021.

605

606 **References**

607

- 608 Anderson S. P., Dietrich W. E., Torres R., Montgomery D. R. and Loague K. (1997)
609 Concentration-discharge relationships in runoff from a steep, unchanneled catchment.
610 *Water Resources Research* **33**, 211–225.
- 611 Bachmair, S., and Weiler, M. (2012). Technical Report on Experimental Hillslope Hydrology,
612 Hydronotes. University of Freiburg, Freiburg, Germany
- 613 Black J. R., Epstein E., Rains W. D., Yin Q. Z. and Casey W. H. (2008) Magnesium-isotope
614 Fractionation During Plant Growth. *Environmental Science & Technology* **42**, 7831–
615 7836.
- 616 Bolou-Bi E. B., Poszwa A., Leyval C. and Vigier N. (2010) Experimental determination of
617 magnesium isotope fractionation during higher plant growth. *Geochimica et*
618 *Cosmochimica Acta* **74**, 2523–2537.
- 619 Bolou-Bi E. B., Vigier N., Poszwa A., Boudot J.-P. and Dambrine E. (2012) Effects of
620 biogeochemical processes on magnesium isotope variations in a forested catchment in the
621 Vosges Mountains (France). *Geochimica et Cosmochimica Acta* **87**, 341–355.

- 622 Bouchez J., Blanckenburg F. von and Schuessler J. A. (2013) Modeling novel stable isotope
623 ratios in the weathering zone. *Am J Sci* **313**, 267–308.
- 624 Brenot A., Cloquet C., Vigier N., Carignan J. and France-Lanord C. (2008) Magnesium isotope
625 systematics of the lithologically varied Moselle river basin, France. *Geochimica et*
626 *Cosmochimica Acta* **72**, 5070–5089.
- 627 Brimhall G. H. and Dietrich W. E. (1987) Constitutive mass balance relations between chemical
628 composition, volume, density, porosity, and strain in metasomatic hydrochemical
629 systems: Results on weathering and pedogenesis. *Geochimica et Cosmochimica Acta* **51**,
630 567–587.
- 631 Campbell D. H., Clow D. W., Ingersoll G. P., Mast M. A., Spahr N. E. and Turk J. T. (1995)
632 Processes Controlling the Chemistry of Two Snowmelt-Dominated Streams in the Rocky
633 Mountains. *Water Resources Research* **31**, 2811–2821.
- 634 Cai, Di; Henehan, Michael; von Blanckenburg, Friedhelm; Uhlig, David (2021): Mg isotopic
635 composition of runoff is buffered by the regolith exchangeable pool. GFZ Data Services.
636 <https://doi.org/10.5880/GFZ.3.3.2021.005>
- 637 Chapela Lara M., Buss H. L., Pogge von Strandmann P. A. E., Schuessler J. A. and Moore O. W.
638 (2017) The influence of critical zone processes on the Mg isotope budget in a tropical,
639 highly weathered andesitic catchment. *Geochimica et Cosmochimica Acta* **202**, 77–100.
- 640 Charlet L. and Sposito G. (1989) Bivalent ion adsorption by an oxisol. *Soil Science Society of*
641 *America Journal* **53**, 691–695.
- 642 Clow D. W. and Mast M. A. (2010) Mechanisms for chemostatic behavior in catchments:
643 Implications for CO₂ consumption by mineral weathering. *Chemical Geology* **269**, 40–
644 51.
- 645 Dessert C., Lajeunesse E., Lloret E., Clergue C., Crispi O., Gorge C. and Quidelleur X. (2015)
646 Controls on chemical weathering on a mountainous volcanic tropical island: Guadeloupe
647 (French West Indies). *Geochimica et Cosmochimica Acta* **171**, 216–237.
- 648 Fahad Z. A., Bolou-Bi E. B., Kohler S. J., Finlay R. D. and Mahmood S. (2016) Fractionation and
649 assimilation of Mg isotopes by fungi is species dependent. *Environ Microbiol Rep.*
- 650 Feger, K.H., 1997. Biogeochemistry of magnesium in forest ecosystems. In *Magnesium*
651 *deficiency in forest ecosystems*. Springer, Dordrecht. pp. 67-99
- 652 Fries D. M., James R. H., Dessert C., Bouchez J., Beaumais A. and Pearce C. R. (2019) The
653 response of Li and Mg isotopes to rain events in a highly-weathered catchment. *Chemical*
654 *Geology* **519**, 68–82.
- 655 Galy A., Yoffe O., E. Janney P., W. Williams R., Cloquet C., Alard O., Halicz L., Wadhwa M.,
656 D. Hutcheon I., Ramon E. and Carignan J. (2003) Magnesium isotope heterogeneity of
657 the isotopic standard SRM980 and new reference materials for magnesium-isotope-ratio
658 measurements. *Journal of Analytical Atomic Spectrometry* **18**, 1352–1356.
- 659 Ganor J., Roueff E., Erel Y. and Blum J. D. (2005) The dissolution kinetics of a granite and its

- 660 minerals—Implications for comparison between laboratory and field dissolution rates.
661 *Geochimica et Cosmochimica Acta* **69**, 607–621.
- 662 Godsey S. E., Kirchner J. W. and Clow D. W. (2009) Concentration–discharge relationships
663 reflect chemostatic characteristics of US catchments. *Hydrological Processes* **23**, 1844–
664 1864.
- 665 Godsey S. E., Hartmann J. and Kirchner J. W. (2019) Catchment chemostasis revisited: Water
666 quality responds differently to variations in weather and climate. *Hydrological Processes*
667 **33**, 3056–3069.
- 668 van der Heijden G., Legout A., Midwood A. J., Craig C.-A., Pollier B., Ranger J. and Dambrine
669 E. (2013) Mg and Ca root uptake and vertical transfer in soils assessed by an in situ
670 ecosystem-scale multi-isotopic (26Mg & 44Ca) tracing experiment in a beech stand
671 (Breuil-Chenue, France). *Plant Soil* **369**, 33–45.
- 672 Hindshaw R. S., Teisserenc R., Le Dantec T. and Tananaev N. (2019) Seasonal change of
673 geochemical sources and processes in the Yenisei River: A Sr, Mg and Li isotope study.
674 *Geochimica et Cosmochimica Acta* **255**, 222–236.
- 675 Hindshaw R. S., Tosca R., Tosca N. J. and Tipper E. T. (2020) Experimental constraints on Mg
676 isotope fractionation during clay formation: Implications for the global biogeochemical
677 cycle of Mg. *Earth and Planetary Science Letters* **531**, 115980.
- 678 James J., Littke K., Bonassi T. and Harrison R. (2016) Exchangeable cations in deep forest soils:
679 Separating climate and chemical controls on spatial and vertical distribution and cycling.
680 *Geoderma* **279**, 109–121.
- 681 Jobbágy E. G. and Jackson R. B. (2001) The distribution of soil nutrients with depth: Global
682 patterns and the imprint of plants. *Biogeochemistry* **53**, 51–77.
- 683 Jobbágy E. G. and Jackson R. B. (2004) The Uplift of Soil Nutrients by Plants: Biogeochemical
684 Consequences Across Scales. *Ecology* **85**, 2380–2389.
- 685 Kim H., Bishop J. K. B., Dietrich W. E. and Fung I. Y. (2014) Process dominance shift in solute
686 chemistry as revealed by long-term high-frequency water chemistry observations of
687 groundwater flowing through weathered argillite underlying a steep forested hillslope.
688 *Geochimica et Cosmochimica Acta* **140**, 1–19.
- 689 Kim H., Dietrich W. E., Thurnhoffer B. M., Bishop J. K. B. and Fung I. Y. (2017) Controls on
690 solute concentration-discharge relationships revealed by simultaneous hydrochemistry
691 observations of hillslope runoff and stream flow: The importance of critical zone
692 structure. *Water Resour. Res.* **53**, 1424–1443.
- 693 Kimmig S. R., Holmden C. and Bélanger N. (2018) Biogeochemical cycling of Mg and its
694 isotopes in a sugar maple forest in Québec. *Geochimica et Cosmochimica Acta*.
- 695 Lang F., Krüger J., Amelung W., Willbold S., Frossard E., Bünemann E. K., Bauhus J., Nitschke
696 R., Kandeler E., Marhan S., Schulz S., Bergkemper F., Schloter M., Luster J., Guggisberg
697 F., Kaiser K., Mikutta R., Guggenberger G., Polle A., Pena R., Prietzel J., Rodionov A.,
698 Talkner U., Meessenburg H., Wilpert K. von, Hölscher A., Dietrich H. P. and Chmara I.

- 699 (2017) Soil phosphorus supply controls P nutrition strategies of beech forest ecosystems
700 in Central Europe. *Biogeochemistry* **136**, 5–29.
- 701 Li W., Beard B. L., Li C. and Johnson C. M. (2014) Magnesium isotope fractionation between
702 brucite [Mg(OH)₂] and Mg aqueous species: Implications for silicate weathering and
703 biogeochemical processes. *Earth and Planetary Science Letters* **394**, 82–93.
- 704 Liu X.-M., Teng F.-Z., Rudnick R. L., McDonough W. F. and Cummings M. L. (2014) Massive
705 magnesium depletion and isotope fractionation in weathered basalts. *Geochimica et*
706 *Cosmochimica Acta* **135**, 336–349.
- 707 Ma L., Teng F.-Z., Jin L., Ke S., Yang W., Gu H.-O. and Brantley S. L. (2015) Magnesium
708 isotope fractionation during shale weathering in the Shale Hills Critical Zone
709 Observatory: Accumulation of light Mg isotopes in soils by clay mineral transformation.
710 *Chemical Geology* **397**, 37–50.
- 711 Maher K., Johnson N. C., Jackson A., Lammers L. N., Torchinsky A. B., Weaver K. L., Bird D.
712 K. and Brown G. E. (2016) A spatially resolved surface kinetic model for forsterite
713 dissolution. *Geochimica et Cosmochimica Acta* **174**, 313–334.
- 714 Markewitz D., Davidson E. A., Figueiredo R. de O., Victoria R. L. and Krusche A. V. (2001)
715 Control of cation concentrations in stream waters by surface soil processes in an
716 Amazonian watershed. *Nature* **410**, 802–805.
- 717 Mavromatis V., Prokushkin A. S., Pokrovsky O. S., Viers J. and Korets M. A. (2014) Magnesium
718 isotopes in permafrost-dominated Central Siberian larch forest watersheds. *Geochimica et*
719 *Cosmochimica Acta* **147**, 76–89.
- 720 Miller E. K., Blum J. D. and Friedland A. J. (1993) Determination of soil exchangeable-cation
721 loss and weathering rates using Sr isotopes. *Nature* **362**, 438–441.
- 722 Montgomery D. R. and Dietrich W. E. (2002) Runoff generation in a steep, soil-mantled
723 landscape. *Water Resources Research* **38**, 7-1-7–8.
- 724 Novak M., Farkas J., Kram P., Hruska J., Stepanova M., Veselovsky F., Curik J., Andronikov A.
725 V., Sebek O., Simecek M., Fottova D., Bohdalkova L., Prechova E., Koubova M. and
726 Vitkova H. (2020a) Controls on $\delta^{26}\text{Mg}$ variability in three Central European headwater
727 catchments characterized by contrasting bedrock chemistry and contrasting inputs of
728 atmospheric pollutants. *PLOS ONE* **15**, e0242915.
- 729 Novak M., Holmden C., Farkas J., Kram P., Hruska J., Curik J., Veselovsky F., Stepanova M.,
730 Kochergina Y. V., Erban V., Andronikov A., Sebek O., Koubova M., Bohdalkova L. and
731 Vitkova H. (2020b) Magnesium and calcium isotope systematics in a headwater
732 catchment underlain by amphibolite: Constraints on Mg–Ca biogeochemistry in an
733 atmospherically polluted but well-buffered spruce ecosystem (Czech Republic, Central
734 Europe). *CATENA* **193**, 104637.
- 735 Novak M., Andronikov A., Kram P., Curik J., Veselovsky F., Stepanova M., Prechova E., Sebek
736 O. and Bohdalkova L. (2021) Time-series of $\delta^{26}\text{Mg}$ values in a headwater catchment
737 reveal decreasing magnesium isotope variability from precipitation to runoff.
738 *Hydrological Processes* **35**, e14116.

- 739 Oh N.-H. and Richter Jr. D. D. (2004) Soil acidification induced by elevated atmospheric CO₂.
740 *Global Change Biology* 10, 1936–1946.
- 741 Opfergelt S., Burton K. W., Georg R. B., West A. J., Guicharnaud R. A., Sigfusson B., Siebert C.,
742 Gislason S. R. and Halliday A. N. (2014) Magnesium retention on the soil exchange
743 complex controlling Mg isotope variations in soils, soil solutions and vegetation in
744 volcanic soils, Iceland. *Geochimica et Cosmochimica Acta* **125**, 110–130.
- 745 Pogge von Strandmann P. A. E., Burton K. W., James R. H., van Calsteren P., Gislason S. R. and
746 Sigfusson B. (2008) The influence of weathering processes on riverine magnesium
747 isotopes in a basaltic terrain. *Earth and Planetary Science Letters* **276**, 187–197.
- 748 Pokharel R., Gerrits R., Schuessler J. A., Frings P. J., Sobotka R., Gorbushina A. A. and von
749 Blanckenburg F. (2018) Magnesium Stable Isotope Fractionation on a Cellular Level
750 Explored by Cyanobacteria and Black Fungi with Implications for Higher Plants.
751 *Environ. Sci. Technol.* **52**, 12216–12224.
- 752 Pokharel R., Gerrits R., Schuessler J. A. and von Blanckenburg F. (2019) Mechanisms of olivine
753 dissolution by rock-inhabiting fungi explored using magnesium stable isotopes. *Chemical
754 Geology* **525**, 18–27.
- 755 Poppe, L.J., Paskevich, V.F., Hathaway, J.C. and Blackwood, D.S., (2001). A laboratory manual
756 for X-ray powder diffraction. US Geological Survey open-file report, 1(041), 1-88.
- 757 Ryu J.-S., Jacobson A. D., Holmden C., Lundstrom C. and Zhang Z. (2011) The major ion,
758 $\delta^{44}/^{40}\text{Ca}$, $\delta^{44}/^{42}\text{Ca}$, and $\delta^{26}/^{24}\text{Mg}$ geochemistry of granite weathering at pH=1 and
759 T=25°C: power-law processes and the relative reactivity of minerals. *Geochimica et
760 Cosmochimica Acta* **75**, 6004–6026.
- 761 Ryu J.-S., Vigier N., Decarreau A., Lee S.-W., Lee K.-S., Song H. and Petit S. (2016)
762 Experimental investigation of Mg isotope fractionation during mineral dissolution and
763 clay formation. *Chemical Geology* **445**, 135–145.
- 764 Saenger C. and Wang Z. (2014) Magnesium isotope fractionation in biogenic and abiogenic
765 carbonates: implications for paleoenvironmental proxies. *Quaternary Science Reviews*
766 **90**, 1–21.
- 767 Salve R., Rempe D. M. and Dietrich W. E. (2012) Rain, rock moisture dynamics, and the rapid
768 response of perched groundwater in weathered, fractured argillite underlying a steep
769 hillslope. *Water Resources Research* 48.
- 770 Schmitt A.-D., Vigier N., Lemarchand D., Millot R., Stille P. and Chabaux F. (2012) Processes
771 controlling the stable isotope compositions of Li, B, Mg and Ca in plants, soils and
772 waters: A review. *Comptes Rendus Geoscience* **344**, 704–722.
- 773 Schott J., Mavromatis V., Fujii T., Pearce C. R. and Oelkers E. H. (2016) The control of
774 carbonate mineral Mg isotope composition by aqueous speciation: Theoretical and
775 experimental modeling. *Chemical Geology* **445**, 120–134.
- 776 Schuessler J. A., Kämpf H., Koch U. and Alawi M. (2016) Earthquake impact on iron isotope
777 signatures recorded in mineral spring water. *Journal of Geophysical Research: Solid*

- 778 *Earth* **121**, 8548–8568.
- 779 Shalev N., Farkaš J., Fietzke J., Novák M., Schuessler J. A., Strandmann P. A. E. P. von and
780 Törber P. B. (2018) Mg Isotope Interlaboratory Comparison of Reference Materials from
781 Earth-Surface Low-Temperature Environments. *Geostandards and Geoanalytical*
782 *Research* **42**, 205–221.
- 783 Sohr J., Uhlig D., Kaiser K., von Blanckenburg F., Siemens J., Seeger S., Frick D. A., Krüger J.,
784 Lang F. and Weiler M. (2019) Phosphorus Fluxes in a Temperate Forested Watershed:
785 Canopy Leaching, Runoff Sources, and In-Stream Transformation. *Front. For. Glob.*
786 *Change* **2**, 85.
- 787 Sprenger M., Seeger S., Blume T. and Weiler M. (2016) Travel times in the vadose zone:
788 Variability in space and time. *Water Resources Research* **52**, 5727–5754.
- 789 Teng F.-Z. (2017) Magnesium Isotope Geochemistry. *Reviews in Mineralogy and Geochemistry*
790 **82**, 219–287.
- 791 Teng F.-Z., Li W.-Y., Rudnick R. L. and Gardner L. R. (2010) Contrasting lithium and
792 magnesium isotope fractionation during continental weathering. *Earth and Planetary*
793 *Science Letters* **300**, 63–71.
- 794 Tipper E. T., Galy A. and Bickle M. J. (2008) Calcium and magnesium isotope systematics in
795 rivers draining the Himalaya-Tibetan-Plateau region: Lithological or fractionation
796 control? *Geochimica et Cosmochimica Acta* **72**, 1057–1075.
- 797 Tipper E. T., Galy A. and Bickle M. J. (2006a) Riverine evidence for a fractionated reservoir of
798 Ca and Mg on the continents: Implications for the oceanic Ca cycle. *Earth and Planetary*
799 *Science Letters* **247**, 267–279.
- 800 Tipper E. T., Galy A., Gaillardet J., Bickle M. J., Elderfield H. and Carder E. A. (2006b) The
801 magnesium isotope budget of the modern ocean: Constraints from riverine magnesium
802 isotope ratios. *Earth and Planetary Science Letters* **250**, 241–253.
- 803 Tipper E. T., Lemarchand E., Hindshaw R. S., Reynolds B. C. and Bourdon B. (2012) Seasonal
804 sensitivity of weathering processes: Hints from magnesium isotopes in a glacial stream.
805 *Chemical Geology* **312–313**, 80–92.
- 806 Trivedi P. and Axe L. (2001) Predicting Divalent Metal Sorption to Hydrous Al, Fe, and Mn
807 Oxides. *Environ. Sci. Technol.* **35**, 1779–1784.
- 808 Uhlig D., Amelung W. and Blanckenburg F. von (2020) Mineral Nutrients Sourced in Deep
809 Regolith Sustain Long-Term Nutrition of Mountainous Temperate Forest Ecosystems.
810 *Global Biogeochemical Cycles* **34**, e2019GB006513.
- 811 Uhlig D. and von Blanckenburg F. (2019) How Slow Rock Weathering Balances Nutrient Loss
812 During Fast Forest Floor Turnover in Montane, Temperate Forest Ecosystems. *Front.*
813 *Earth Sci.* **7**.
- 814 Uhlig D., Schuessler J. A., Bouchez J., Dixon J. L. and von Blanckenburg F. (2017) Quantifying
815 nutrient uptake as driver of rock weathering in forest ecosystems by magnesium stable

- 816 isotopes. *Biogeosciences* **14**, 3111–3128.
- 817 Wimpenny J., Burton K. W., James R. H., Gannoun A., Mokadem F. and Gíslason S. R. (2011)
818 The behaviour of magnesium and its isotopes during glacial weathering in an ancient
819 shield terrain in West Greenland. *Earth and Planetary Science Letters* **304**, 260–269.
- 820 Wimpenny J., Colla C. A., Yin Q.-Z., Rustad J. R. and Casey W. H. (2014) Investigating the
821 behaviour of Mg isotopes during the formation of clay minerals. *Geochimica et*
822 *Cosmochimica Acta* **128**, 178–194.
- 823 Wimpenny J., Gíslason S. R., James R. H., Gannoun A., Pogge Von Strandmann P. A. E. and
824 Burton K. W. (2010) The behaviour of Li and Mg isotopes during primary phase
825 dissolution and secondary mineral formation in basalt. *Geochimica et Cosmochimica*
826 *Acta* **74**, 5259–5279.
- 827 Brady N. C. and Weil R. R. (2008) *The Nature and Properties of Soils.*, Prentice Hall.
- 828 Yu Z., Chen H. Y. H., Searle E. B., Sardans J., Ciais P., Peñuelas J. and Huang Z. (2020) Whole
829 soil acidification and base cation reduction across subtropical China. *Geoderma* **361**,
830 114107.
- 831
- 832